Available online at www.sciencedirect.com
SCIENCE DIRECT®
Journal of Magnetic Resonance 169 (2004) 60–67
JMR Journal of Magnetic Resonance
www.elsevier.com/locate/jmr

Combined relaxation and displacement experiment: a fast method to acquire T_2, diffusion and velocity maps

Bertram Manz*

Arbeitsgruppe Magnetische Resonanz, Fraunhofer-Institut für Biomedizinische Technik, Ensheimer Straße 48, 66386 St. Ingbert, Germany

Received 20 February 2004; revised 6 April 2004
Available online 27 April 2004

Abstract

A fast method for quantitative imaging of T_2 and displacement (flow and diffusion) is presented. The pulse sequence combines multi-PGSE NMR with multi-echo acquisition and compensates for flow effects in the read gradient and diffusion during multi-echo trains. The impact of the gradient pulses in a multi-echo train on the signal phase and amplitude is discussed. It is shown that separate T_2 and displacement images with microscopic resolution can be obtained within minutes. The capability for 3D flow imaging is demonstrated. The sequence is then used to investigate forced detachment of a biofilm in a tube.

Keywords: Flow; Diffusion; T_2 relaxation; Fast imaging; Biofilm

1. Introduction

Compared to other non-invasive imaging methods, one of the most distinguishing features of MRI is the possibility to measure parameter-weighted or parameter images [1–3]. Such parameters include longitudinal and transverse relaxation, diffusion, chemical shift, and molecular order, just to name a few. A parameter image can reveal structures in the sample, which may not be apparent in a normal proton density image. A standard procedure to measure a parameter image is to acquire a series of parameter-weighted images and apply a fitting function to each image voxel in order to extract the parameter of interest. Due to this, the acquisition of such parameter images is time consuming, and not suitable for dynamic systems or three-dimensional imaging.

Fast imaging techniques based on low-angle excitation, like FLASH [4] or SSFP [5], enable a fast image acquisition, but suffer from relatively poor signal-to-noise ratio as well as T_2^* signal attenuation, which is a serious problem for microimaging applications.

Other fast imaging techniques such as RARE [6] or EPI [7], and their hybrids [8–18], are extremely useful for proton density and velocity imaging, even with microscopic resolution. The idea is to sample multiple lines in k-space with a single excitation by signal refocusing using spin-echoes or gradient echoes and incrementing the phase encoding gradient between successive echoes. However, because the echoes are all acquired with different echo times, the resulting images suffer from T_2 or T_2^* contrast, which makes these methods less suitable for the measurement of T_2 maps.

A different approach for the fast acquisition of T_2 maps has been introduced by Edzes et al. [19]. Like the RARE technique, it is based on a multi-echo train, but here subsequent echoes are used for T_E-weighting, and a normal spin-warp is employed for phase encoding. The authors point out that due to diffusive signal loss in the applied read gradient an apparent relaxation time T_2'', which is shorter than T_2, is measured using such a multi-echo sequence. For voxel sizes larger than 100 μm, the difference between T_2'' and T_2 is negligible, but becomes more important as the pixel size decreases. Ultimately, as the resolution and therefore the read gradient increases, the diffusive signal attenuation dictates the value of T_2'', and any information about the intrinsic value of

* Fax: +49-6894-980400.
E-mail address: bertram.manz@ibmt.fraunhofer.de.

1090-7807/$ - see front matter © 2004 Elsevier Inc. All rights reserved.
doi:10.1016/j.jmr.2004.04.003

T_2 is lost [2,19,20]. By introducing two separate delays in the echo cycle, it is possible to compensate for diffusion effects in a T_2 imaging experiment [21], or to compensate for T_2-effects in a diffusion imaging experiment [22].

The imaging sequence reported in this paper describes how a new variant of the multi-echo sequence avoids this drawback and can be applied to yield a high resolution map of both intrinsic T_2 and displacement. We have termed this sequence COMbined Relaxation and Displacement Experiment (COMRADE). This sequence is particularly useful for studying systems where both T_2 and displacement images are required. Examples of such systems are brain lesions [23–26], plant material [16,27–30], and biofilms [31–36], just to name a few.

In this study, the COMRADE sequence will be demonstrated on three systems: (i) a static phantom sample containing liquids with different T_2 and self-diffusion coefficients, (ii) water flowing through a step contraction, and (iii) a study on forced detachment of biofilm in a tube reactor.

2. Theory

A schematic diagram of the COMRADE pulse sequence is shown in Fig. 1, where pulse, and delay times are defined. The experiment is based on a multi-echo sequence similar to the RARE experiment. However, only every second echo is used for data acquisition. This allows easy flow encoding while retaining the overall symmetry of the pulse sequence. Also, as will be shown in the next paragraph, the read gradient of every second echo is naturally flow compensated, which is of great advantage when dealing with fast flow velocities. For the same reason, the slice gradient is flow compensated as well.

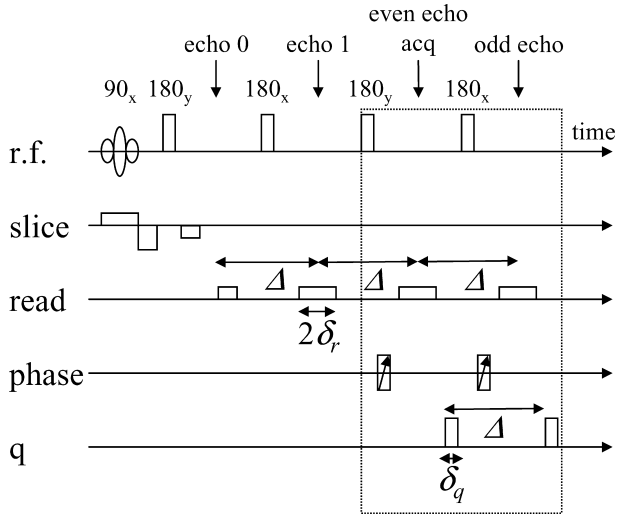

Fig. 1. A schematic diagram of the COMRADE pulse sequence. The arrows mark the positions of spin echoes, and the dashed box indicates the multiple echo acquisition loop. The phase encoding gradient, which is incremented between scans like in single echo spin warp imaging, is applied to even echoes and unwound again for odd echoes. The displacement encoding q-gradient may be along any direction.

It should be noted that the gradient cycles considered here are similar to the cycles applied by Callaghan and Stepišnik [37]. However, these authors perform a frequency-domain analysis of the echo signal by varying the delay between gradient pulses and keeping the length of the echo train constant. As a contrast, our suggested experiment is a time-domain analysis with incrementing evolution time.

We will now calculate the effect of flow, unrestricted, diffusion and transverse relaxation on the signal intensity during the nth echo ($n = 1, 2, \ldots$) in the multi-echo train shown in Fig. 1.

2.1. Flow

To calculate the effects of the gradient pulses on the signal phase, it is convenient to define the effective gradient $g^*(t)$, which takes account of the influence of RF pulses on the spin phase [2]. These, along with the zeroth moment of the magnetic field gradient $M_0(t) = \int_0^t g^*(t')\mathrm{d}t'$, are shown in Fig. 2 for gradients along the read, and displacement encoding (q) direction. For the read gradient, a gradient echo, and therefore signal refocusing, occurs at echo times $t_e = n\Delta (n = 1, 2, \ldots)$ where $M_{0,r}(t) = 0$.

The phase shift ϕ of a spin moving with velocity component v_0 along the gradient direction is given by [38]

$$\phi(t) = \gamma v_0 \int_0^t g^*(t')t'\mathrm{d}t'. \tag{1}$$

The phase shift $\phi_r(n\Delta)$ due to the read gradient can be calculated at the echo point as:

$$\phi_r(n\Delta) = 0 \text{ for } n \text{ even}, \tag{2}$$

$$\phi_r(n\Delta) = \gamma v_0 g_r \delta_r(\Delta - \delta_r) \text{ for } n \text{ odd}. \tag{3}$$

This implies that even echoes experience no phase shift due to constant flow along the read gradient direction.

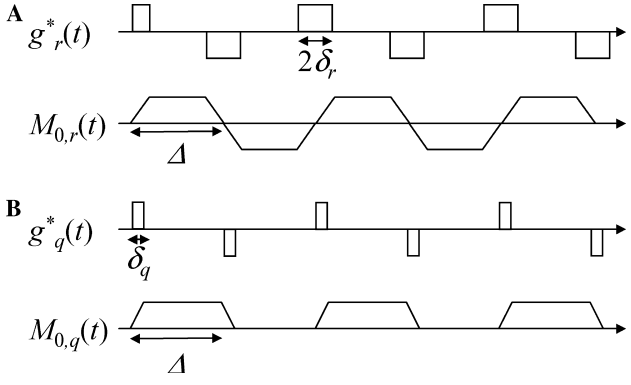

Fig. 2. The effective gradient g^* and the zeroth moment M_0 of the read (A) and displacement (B) encoding gradient for the pulse sequence shown in Fig. 1.

Similarly, Eq. (1) yields the phase shift due to the displacement encoding gradient at even echoes:

$$\phi_q(2n\Delta) = n\gamma v_0 g_q \delta_q \Delta. \tag{4}$$

This relationship is similar to the phase shift of moving spins in a PGSE experiment. The impact of Eq. (4) is that the phase shift can be sampled through the acquisition of a number of echoes in the same way as through stepping the gradient strength in a conventional dynamic imaging experiment [39]. Because the acquisition of all displacement encoding steps occurs within one scan, the overall acquisition time can be greatly reduced.

2.2. Diffusion

In the case of isotropic unrestricted diffusion with coefficient D, the echo attenuation function E is given by [40]:

$$E(t) = \exp\left[-D\gamma^2 \int_0^t \left(\int_0^{t'} g^*(t'')\mathrm{d}t''\right)^2 \mathrm{d}t'\right]. \tag{5}$$

The inner integral equals the zeroth moment $M_0(t')$, which is shown in Fig. 2 for both read, and displacement encoding gradients. Inserting these values in Eq. (5) yields at the echo points $t = 2n\Delta$:

$$E(2n\Delta) = \exp\left(-2nD\gamma^2 g_r^2 \delta_r^2((\Delta - \delta_r) - \delta_r/3)\right) \quad \text{due to the read gradient,} \tag{6}$$

$$E(2n\Delta) = \exp\left(-nD\gamma^2 g_q^2 \delta_q^2(\Delta - \delta_q/3)\right) \quad \text{due to the displacement gradient.} \tag{7}$$

For $n = 1$, Eq. (7) reduces to the well-known Stejskal–Tanner equation [41] for a simple PGSE experiment. The impact of Eqs. (6) and (7) is that unrestricted diffusive effects lead to a multiplication of the attenuation factors so that a multi-echo PGSE sequence produces exactly n times the attenuation of a single PGSE experiment [19].

2.3. Transverse relaxation

In this treatment we assume that the time Δ between subsequent 180° pulses is short enough that signal attenuation due to internal magnetic field gradients can be neglected. Then the echo attenuation function due to transverse relaxation is given at time t_e by [42]:

$$E(t_e) = \exp(-t_e/T_2). \tag{8}$$

The total attenuation of the echo signal due to diffusion and T_2 relaxation is then a combination of Eqs. (6)–(8):

$$E(2n\Delta) = \exp\left(-2nD\gamma^2 g_r^2 \delta_r^2((\Delta - \delta_r) - \delta_r/3)\right) \times \exp\left(-nD\gamma^2 g_q^2 \delta_q^2(\Delta - \delta_q/3)\right) \times \exp(-2n\Delta/T_2). \tag{9}$$

From Eq. (9) it is evident that both D and T_2 cannot be measured with a single multi-echo experiment. We suggest therefore to sample the signal in two scans with the same pulse sequence and parameters. The first scan is applied with $g_q = 0$ and measures $E_0 = E(2n\Delta, g_q = 0)$. For the second scan, which then measures $E_g = E(2n\Delta, g_q)$, g_q is chosen to supply sufficient attenuation according to Eq. (7). The signal ratio of both scans is independent of g_r and T_2:

$$\frac{E_g}{E_0} = \exp\left(-nD\gamma^2 g_q^2 \delta_q^2(\Delta - \delta_q/3)\right), \tag{10}$$

from which D can be easily calculated.

3. Experimental

3.1. Diffusion and relaxation time imaging

All experiments were performed on a Bruker Avance 400 NMR spectrometer with microimaging equipment. The maximum achievable gradient is $1\,\mathrm{T\,m^{-1}}$. To test the COMRADE sequence, a phantom consisting of different liquids was constructed. The liquids are chosen to have different values of T_1, T_2, diffusion coefficient and chemical shift. Such a phantom can be used to teach students the basics of MR contrast. Example images of the phantom with different parameter weightings have been made available through the internet [43]. A schematic of the phantom is shown in Fig. 3.

The COMRADE pulse sequence relies, like most multi-echo sequences, on a complete refocusing of the signal by the 180° pulses. Small deviations in the flip angle can lead to additional signal attenuation, and a mixture of the quadrature components [44]. The latter effect is more serious, as it creates ghosting artefacts in the images. To suppress these artefacts, several measures were taken. First, a relatively large r.f. coil (25 mm i.d.) was used so that the homogeneous region covers most of the sample. Second, composite refocusing pulses were applied, as described by Manz et al. [15]. Third, it was found that a 2-step (x, y) phase cycling [44] of the refocusing pulses brought further improvement.

The phase encoding gradient, which was incremented between scans like in single echo spin warp imaging, was applied prior to reading each even echo. A reverse phase encode step was then applied during the following odd echo to remove the phase memory of the signal prior to the next data collection. This phase encoding scheme is similar to the method used by Mulkern et al. [45], where the reverse phase encoding step is applied directly after echo collection. However, it was found that the method used here is less likely to produce image artefacts, especially for flowing systems.

A series of eight out of 16 images of the phantom sample acquired with the COMRADE sequence is

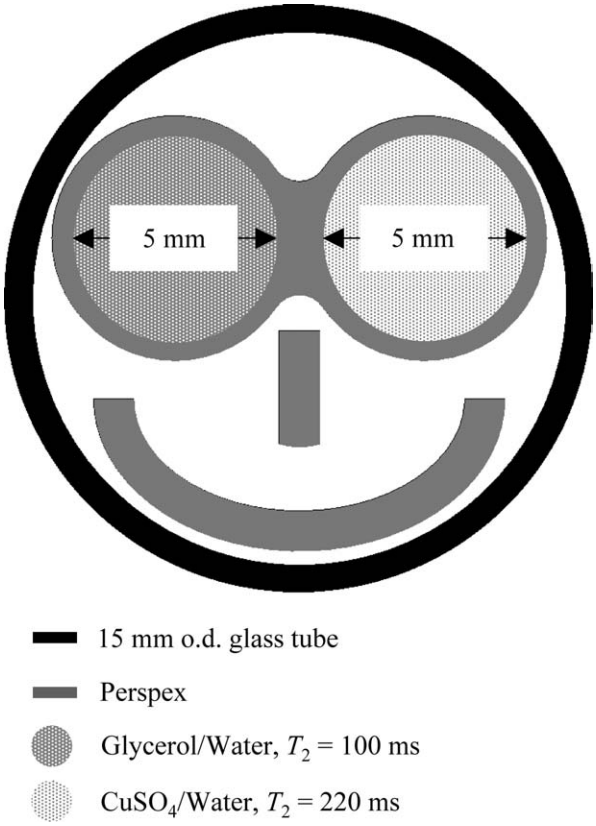

Fig. 3. A schematic of the phantom sample. The perspex structure is placed inside a 15 mm NMR tube, the void space is filled with tap water. One hole in the perspex structure is filled with a 5 mM $CuSO_4$/water solution, while the other hole contains a water/glycerol mixture. The fluids in this sample show contrast in T_1, T_2 chemical shift and self-diffusion.

shown in Fig. 4 without (A) and with q-gradient (B). Because of the complete signal refocusing all images are artefact free. Experimental parameters were: $T_r = 1.5$ s, $\Delta = 6$ ms, $\delta_r = \delta_q = 0.82$ ms, $g_r = 0.16\,\mathrm{T\,m^{-1}}$, $g_q = 0$ (A) or $0.5\,\mathrm{T\,m^{-1}}$ (B). The overall acquisition time for each series was 6.5 min, which is around 10 times faster than the acquisition of 16 separate images with different diffusion or T_2 weighting.

3.2. Flow imaging

The COMRADE sequence was then applied to measure flow velocities. A simple geometry with an interesting flow pattern is the step contraction, which has been investigated in detail by Callaghan and Xia [46]. The exact details of the flow profile in such a cell shall not be discussed here, because the purpose of this experiment is not to verify previous results, but to demonstrate the COMRADE sequence. The flow cell was made out of a 8 mm i.d. (10 mm o.d.) glass tube inside a 9 mm i.d. plastic tube, as shown in Fig. 5. Tap water was pumped through the cell at a constant flow rate of 0.3 l per hour using a Pharmacia P-1 peristaltic pump. Pulsations in the flow were dampened by pumping the fluid between two reservoirs at different levels, as described previously [34]. To demonstrate the capability for three-dimensional imaging, a 9 mm thick horizontal slab was excited, and a second 3D phase encoding gradient was applied in the slice direction. A series of 16 echo images was acquired with $g_q = 0.4\,\mathrm{T\,m^{-1}}$ along the axial direction. Subsequent Fourier inversion in three spatial and the q dimension yielded a three-dimensional map of propagators. The flow velocity in each voxel was

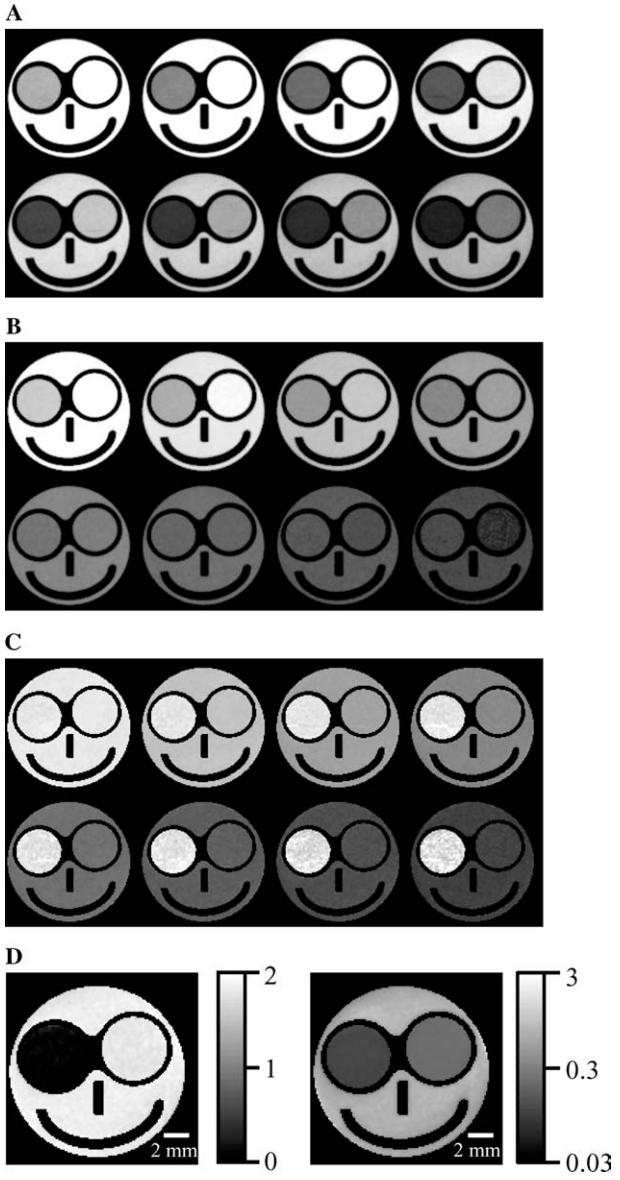

Fig. 4. A series of COMRADE images of the phantom sample without (A) and with (B) q-gradient applied. The images were acquired with 15 mm field of view, 1 mm slice thickness, and 128×128 points. Every second out of 16 echoes is shown. (C) The images shown in (B) divided by the images shown in (A). The images in this sequence are only weighted by self-diffusion. (D) Images of the self-diffusion coefficient (left, scale in $10^{-9}\,\mathrm{m^2\,s^{-1}}$) and T_2 (right, logarithmic scale in s) obtained from the images shown in (A–C). See text for details.

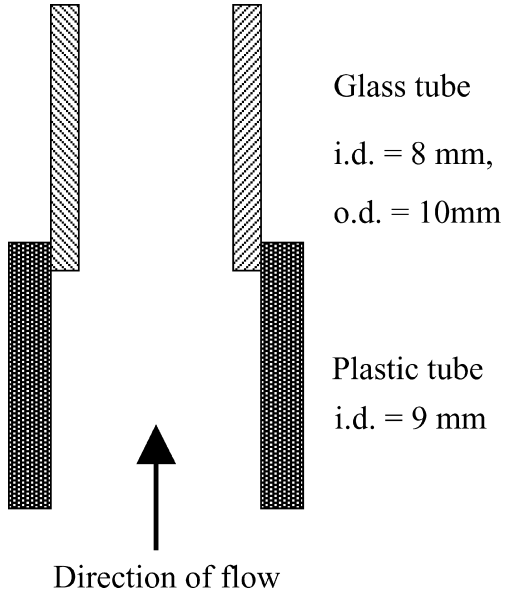

Fig. 5. A schematic of the flow cell. Tap water was pumped through the cell at a flow rate of $0.31\,h^{-1}$.

obtained through the method described by Callaghan and Xia [39]. Experimental parameters were: $T_r = 1.5\,s$, $\Delta = 10\,ms$, $\delta_r = \delta_q = 0.82\,ms$, $g_r = 0.23\,T\,m^{-1}$, $g_q = 0.4\,T\,m^{-1}$, with an overall acquisition time of 4.6 hours per image.

3.3. Flow and relaxation time imaging

Forced detachment was studied on a biofilm sample which was cultivated at room temperature in a 7 mm i.d. tube reactor at a Reynolds number of 3000. Once the film reached a thickness of approximately 1 mm, the tube was transferred to the NMR spectrometer and connected to a flow loop as described by Manz et al. [34]. Tap water was pumped through the cell at a constant flow rate of $0.31\,h^{-1}$ using a Pharmacia P-1 peristaltic pump. A series of 16 echo images was acquired with the COMRADE sequence without and with q-gradient applied along the axial direction. Experimental parameters were: $T_r = 2\,s$, $\Delta = 10\,ms$, $\delta_r = \delta_q = 1.35\,ms$, $g_r = 0.23\,T\,m^{-1}$, $g_q = 0$ or $0.15\,T\,m^{-1}$. The overall acquisition time for each series was 8.25 min.

Detachment was achieved by inserting a gear pump into the flow loop and increasing the flow rate until the desired Reynolds number was reached inside the tube. This flow rate was maintained for 2 min, after which the flow rate was controlled again by the peristaltic pump, and the next experiment was carried out.

4. Results and discussion

4.1. Diffusion and relaxation time imaging

To obtain the local values of T_2 and D, two series of COMRADE images of the phantom sample were acquired, one with $g_q = 0$ (image A) and another with $g_q = 0.5\,T\,m^{-1}$ (image B). Image A serves as a reference scan in order to eliminate signal attenuation due to T_2 relaxation and the read gradient g_r according to Eq. (10). Each echo of image B was divided by the corresponding echo of image A yielding an image of attenuation factors (image C). The series of echoes of images A, B, and C are shown in Figs. 4 A–C. The value of D was calculated in each voxel through a least squares fit of Eq. (10) to image C. Finally, using this value of D,

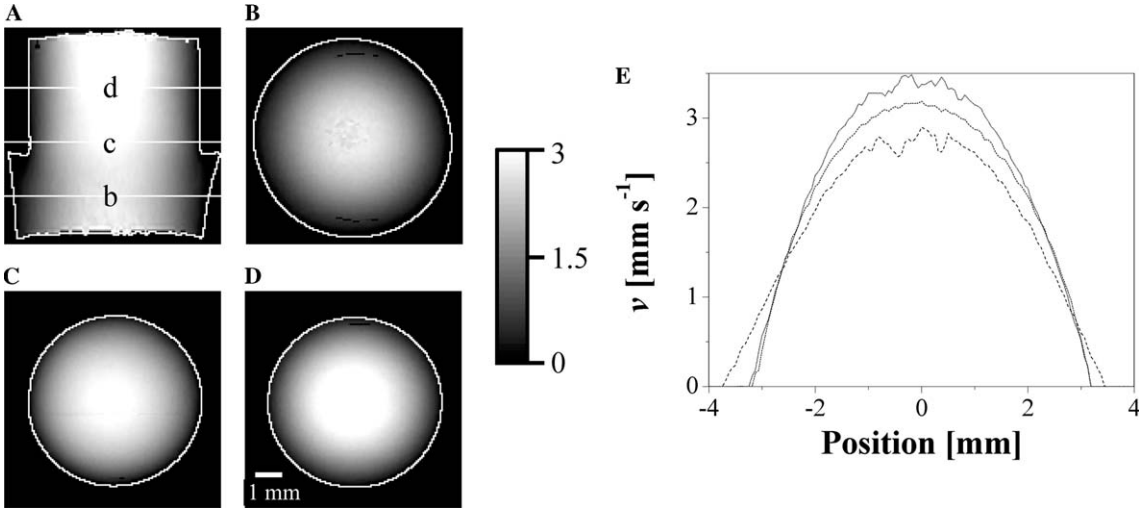

Fig. 6. Selected slices through the three-dimensional velocity image of the flow cell. (A) A vertical slice through the centre of the cell. The positions of the horizontal slices (B–D) are marked. The velocity image was acquired with a 10 mm field of view, 128×128 points horizontally, and 64 points along the axial direction. The colorbar represents the velocity scale and is in $mm\,s^{-1}$. (E) Velocity profiles through the centre of the images (B) – –, (C) - -, and (D) ··.

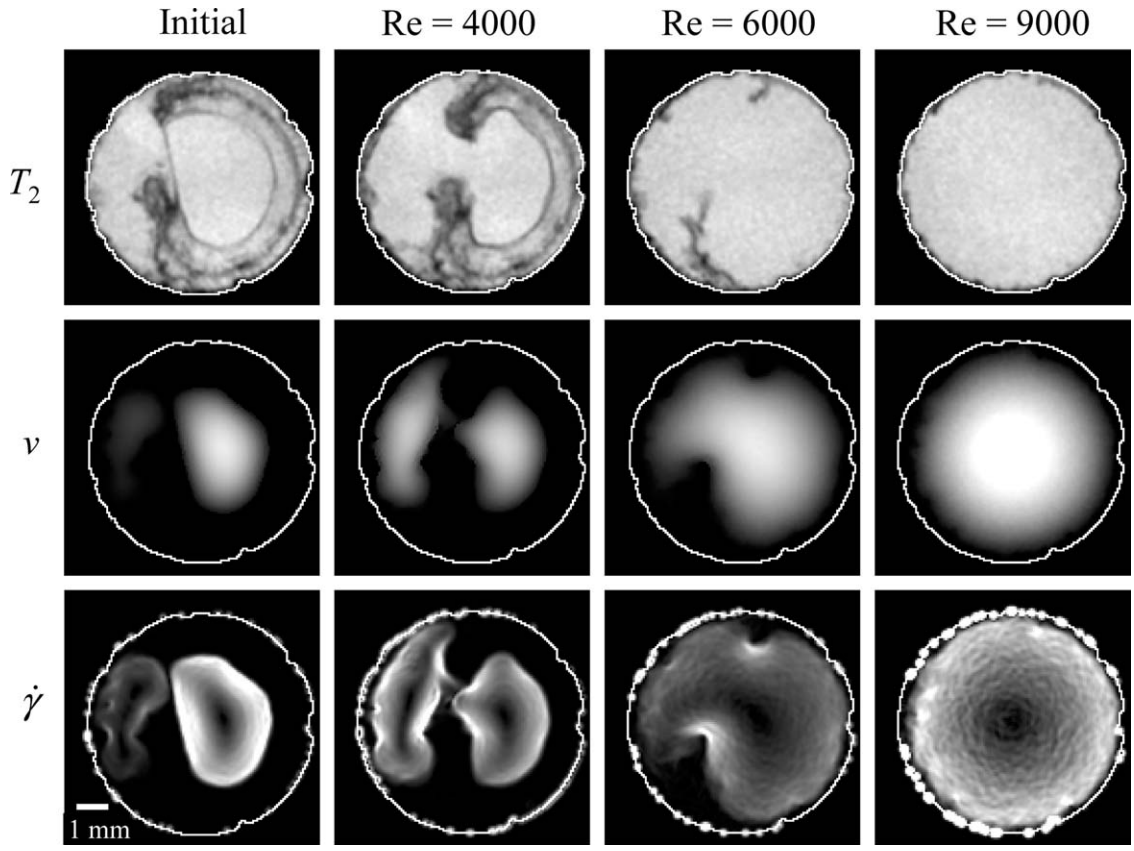

Fig. 7. Images of the biofilm sample acquired with the COMRADE sequence after different detachment velocities. All images were acquired with a 8 mm field of view, 1 mm slice thickness and 128×128 points. Note that the greyscale varies for different velocity and shear rate images. See text for details.

Eq. (9) was fitted to image A in order to compute an image of T_2 values. The spatially resolved maps of D and T_2 obtained in this way are shown in Fig. 4 D. We note that the values of D and T_2 measured with COMRADE agree very well with conventional experiments (error less than 10%).

4.2. Flow imaging

Fig. 6 shows a vertical (A) and three selected horizontal (B–D) slices through the three-dimensional velocity image of water flowing through the step contraction described in the previous section. The velocity profiles through the centre of the flow cell are shown in Fig. 6 (E). These images, as well as the profiles, agree well with previously published results from two-dimensional velocity images [46].

It has been shown that the signal phase shift in a PGSE experiment is not only given by the local constant velocity, but local acceleration and higher time derivatives of velocity may contribute to the phase shift as well [38,47]. Such additional phase shifts may lead to increased signal attenuation in a multi-echo PGSE sequence and can be wrongly assigned to an increased self-diffusion coefficient or a reduced T_2 value. However, in the systems investigated here, the transverse flow velocity components are approximately one order of magnitude smaller than the axial component [36,46]. The local accelerations, which are in stationary flowing systems purely due to spatial velocity fluctuations, are therefore relatively small. This was verified by subsequent analysis of T_2 values in the step contraction, which showed no spatial variation of T_2. Therefore, the effect of time derivatives of the local velocity can be neglected for the systems investigated in this study.

4.3. Flow and relaxation time imaging

Having demonstrated the capability of the COMRADE sequence to investigate displacement and transverse relaxation in model systems, we apply this method to study forced detachment in biofilm systems. The results presented here are part of a larger study which will be published elsewhere.

The images of the biofilm sample are shown in Fig. 7. At each stage a T_2 (top row) and a velocity map (middle row) was recorded. The T_2 maps yield information about the biofilm structure, while from the velocity maps the local shear rates $\dot{\gamma} = |\mathrm{grad}(v)|$, which are a measure for the hydrodynamic forces acting on the biofilm surface,

can be calculated (bottom row). The greyscale of T_2 values ranges from 60 to 160 ms. All velocity images were recorded with the same flow rate of $0.3\,l\,h^{-1}$. Between subsequent images a larger region becomes available for the fixed flow to occur in due to detachment. As a consequence, the average fluid flow velocity decreases with increasing void space in the image sequence from left to right. To preserve a similar contrast in all velocity and shear rate images, the greyscale is different for all images. The velocity values shown in Fig. 7 range from left to right between 0 and $20\,mm\,s^{-1}$ (14,8,5), while the values for the shear rate range from 0 to $25\,s^{-1}$ (20,10,4), respectively.

From the initial T_2 image it can be seen that the biofilm has grown in two layers on the right side and is already detached from the left wall. A thin skin splits the bulk fluid into two compartments. This becomes more evident from the initial flow image, which shows that the water transport occurs mainly in the compartment close to the centre of the reactor. The image of the initial shear rate shows that the hydrodynamic forces are particularly high near this skin in the centre of the cell. Therefore it is of no surprise that this skin is washed away in the first detachment experiment (Fig. 7, second column). Two finger-like biofilm structures, which divide the flow image into two areas of convective transport, reach towards the centre of the reactor. The shear rate is now particularly high near these "fingers." Increasing the flow rate for detachment further results in most of the biofilm being washed away (Fig. 7 third column). Finally, after flushing at the highest available flow rate, only an approximately 100 μm thin biofilm layer remains attached to the reactor wall. The flow is essentially unrestricted, yielding the well-known parabolic velocity profile in the tube. The results of such experiments can be of great value in order to verify models for biofilm detachment [48–53].

5. Conclusions

In this contribution a novel multi-echo technique for the fast measurement of T_2 and displacement images has been presented. It has been shown that two-dimensional parameter maps of fluctuating systems can be obtained with microscopic resolution within minutes, which is approximately one order of magnitude faster than using the conventional method. Three-dimensional maps of stationary systems can be measured within reasonable times using the same method.

The COMRADE sequence has been applied to study forced detachment in a biofilm system. It could be shown that detachment occurs preferably at places on the biofilm surface, where the hydrodynamic shear forces are particularly high.

The data presented here suggest the robustness of the technique and therefore make it a favourable tool for applications where fast two- or three-dimensional contrast imaging methods are needed, for example in chemical engineering, or biomedical research.

Acknowledgments

The author wishes to thank Professor Harald Horn for supplying the biofilm sample and suggesting the detachment experiment. He also thanks Dr. Frank Volke for his advice and critically reading the manuscript. Martin Benecke's construction of the phantom sample is highly appreciated.

References

[1] P. Mansfield, P.G. Morris, NMR Imaging in Biomedicine, Academic Press, New York, 1982.
[2] P.T. Callaghan, Principles of Nuclear Magnetic Resonance Microscopy, Clarendon Press, Oxford, 1991.
[3] R. Kimmich, NMR: Tomography, Diffusometry, Relaxometry, Springer-Verlag, Heidelberg, 1997.
[4] A. Haase, J. Frahm, D. Matthaei, W. Hänicke, K.-D. Merboldt, FLASH imaging. rapid NMR imaging using low flip-angle pulses, J. Magn. Reson. 67 (1986) 258–266.
[5] M.L. Gyngell, The application of steady-state free precession in rapid 2DFT NMR imaging: FAST and CE-FAST sequences, J. Magn. Reson. Imaging 6 (1988) 415–419.
[6] J. Hennig, A. Nauerth, H. Friedburg, RARE imaging—a fast imaging method for clinical MR, Magn. Reson. Med. 3 (1986) 823–833.
[7] P. Mansfield, Multi-planar image formation using NMR spin echoes, J. Phys. C. Sol. St. Phys. 10 (1977) L55.
[8] P. Mansfield, B. Issa, Fluid transport in porous rocks. I. EPI studies and a stochastic model of flow, J. Magn. Reson. A 122 (1996) 137–148.
[9] A.M. Peters, P.S. Robyr, R.W. Bowtell, P. Mansfield, Echo-planar microscopy of porous rocks, J. Magn. Reson. Imaging 14 (1996) 875–877.
[10] F. Hennel, Modification of the Carr-Purcell sequence for single-shot echo-planar imaging, Magn. Reson. Med. 26 (1992) 116–121.
[11] D.N. Guilfoyle, P. Mansfield, K.J. Packer, Fluid flow measurement in porous media by echo-planar imaging, J. Magn. Reson. 97 (1992) 342–358.
[12] D.N. Guilfoyle, B. Issa, P. Mansfield, Rapid volumetric NMR imaging of fluids in porous solids using a 3D π-EPI (PEPI) hybrid, J. Magn. Reson. A 119 (1996) 151–156.
[13] K. Oshio, F.A. Jolesz, P.S. Melki, R.V. Mulkern, T_2-weighted thin-section imaging with the multislab three-dimensional RARE technique, J. Magn. Reson. Imaging 1 (1991) 695–700.
[14] A.M. Peters, R. Bowtell, Resolution in high field echo planar microscopy, J. Magn. Reson. 137 (1999) 196–205.
[15] B. Manz, P.S. Chow, L.F. Gladden, Echo-planar imaging of porous media with spatial resolution below 100 μm, J. Magn. Reson. 136 (1999) 226–230.
[16] T.W.J. Scheenen, D. van Dusschoten, P.A. De Jager, H. van As, Microscopic displacement imaging with pulsed field gradient turbo spin-echo NMR, J. Magn. Reson. 142 (2000) 207–215.

[17] A.J. Sederman, M.D. Mantle, L.F. Gladden, Single excitation multiple Image RARE (SEMI-RARE): ultra fast imaging of static and flowing systems, J. Magn. Reson. 161 (2003) 15–24.
[18] A.J. Sederman, M.D. Mantle, C. Buckley, L.F. Gladden, MRI technique for measurement of velocity vectors, acceleration, and autocorrelation functions in turbulent flow, J. Magn. Reson. 166 (2004) 182–189.
[19] H.T. Edzes, D. van Dusschoten, H. van As, Quantitative T2 imaging of plant tissues by means of multi-echo MRI microscopy, J. Magn. Reson. Imaging 16 (1998) 185–196.
[20] C.J. Rofe, J. van Noort, P.J. Back, P.T. Callaghan, NMR Microscopy using large, pulsed magnetic-field gradients, J. Magn. Reson. B 108 (1995) 125–136.
[21] R. Deichmann, H. Adolf, E. Kuchenbrod, U. Nöth, C. Schwarzbauer, A. Haase, Compensation of diffusion effects in T2 measurements, Magn. Reson. Med. 33 (1995) 113–115.
[22] T.J. Norwood, S.L. Duce, L.D. Hall, A Robust method for diffusion-weighted NMR imaging, J. Magn. Reson. A 102 (1993) 370–374.
[23] M.A. Jacobs, R.A. Knight, H. Soltanian-Zadeh, Z.G. Zheng, A.V. Goussev, D.J. Peck, J.P. Windham, M. Chopp, Unsupervised segmentation of multiparameter MRI in experimental cerebral ischemia with comparison to T_2, diffusion, and ADC MRI parameters and histopathological validation, J. Magn. Reson. Imaging 11 (200) 425–437.
[24] M.G. Lansberg, V.N. Thijs, M.W. O'Brien, J.O. Ali, A.J. de Crespigny, D.C. Tong, M.E. Moseley, G.W. Albers, Evolution of apparent diffusion coefficient, diffusion-weighted, and T2-weighted signal intensity of acute stroke, Am. J. Neuroradiol. 22 (2001) 637–644.
[25] N. van Bruggen, B.M. Cullen, M.D. King, M. Doran, S.R. Williams, D.G. Gadian, J.E. Cremer, T2- and diffusion-weighted magnetic resonance imaging of a focal ischemic lesion in rat brain, Stroke 23 (1992) 576–582.
[26] H.B. Verheul, J.W. Berkelbach van der Sprenkel, C.A. Tulleken, K.S. Tamminga, K. Nicolay, Temporal evolution of focal cerebral ischemia in the rat assessed by T_2-weighted and diffusion-weighted magnetic resonance imaging, Brain Topogr. 5 (1992) 171–176.
[27] P.T. Callaghan, C.J. Clark, L.C. Forde, Use of static and dynamic NMR microscopy to investigate the origins of contrast in images of biological tissues, Biophys. Chem. 50 (1994) 225–235.
[28] T.W.J. Scheenen, D. van Dusschoten, P.A. De Jager, H. van As, Quantification of water transport in plants with NMR imaging, J. exp. Bot. 51 (2000) 1751–1759.
[29] M. Rokitta, U. Zimmermann, A. Haase, Fast NMR flow measurements in plants using FLASH imaging, J. Magn. Reson. 137 (1999) 29–32.
[30] H. Schneider, B. Manz, M. Westhoff, S. Mimietz, M. Szimtenings, T. Neuberger, C. Faber, G. Krohne, A. Haase, F. Volke, U. Zimmermann, The impact of lipid distribution, composition and mobility on xylem water refilling of the resurrection plant *Myrothamnus flabellifolia*, New Phytologist 159 (2003) 487–505.
[31] E.E. Beuling, D. van Dusschoten, P. Lens, J.C. van denHeuvel, H. van As, S.P.P. Ottengraf, Characterization of the diffusive properties of biofilms using pulsed field gradient-nuclear magnetic resonance, Biotechnol. Bioeng. 60 (1998) 283–291.
[32] B.C. Hoskins, L. Fevang, P.D. Majors, M.M. Sharma, G. Georgiou, Selective imaging of biofilms in porous media by NMR relaxation, J. Magn. Reson. 139 (1999) 67–73.
[33] Z. Lewandowski, S.A. Altobelli, E. Fukushima, NMR and microelectrode studies of hydrodynamics and kinetics in biofilms, Biotech. Prog. 9 (1993) 40–45.
[34] B. Manz, F. Volke, D. Goll, H. Horn, Measuring local flow velocities and biofilm structure in biofilm systems with magnetic resonance imaging (MRI), Biotechnol. Bioeng. 84 (2003) 424–432.
[35] P.N.L. Lens, H. van As, Use of ^{1}H NMR to study transport processes in biofilms, in: P. Lens, A.P. Moran, T. Mahony, P. Stoodley, V. O'Flaherty (Eds.), Biofilms in Medicine, Industry and Environmental Biotechnology: Characteristics, Analysis and Control, IWA Publishing, 2003, pp. 285–307.
[36] J.D. Seymour, S.L. Codd, E.L. Gjersing, P.S. Stewart, Magnetic resonance microscopy of biofilm structure and impact on transport in a capillary bioreactor, J. Magn. Reson. 167 (2004) 322–327.
[37] P.T. Callaghan, J. Stepišnik, Frequency-domain analysis of spin motion using modulated-gradient NMR, J. Magn. Reson. A 117 (1995) 118–122.
[38] J.M. Pope, S. Yao, Quantitative NMR imaging of flow, Concept Magn. Reson. 5 (1993) 281–302.
[39] P.T. Callaghan, Y. Xia, Velocity and diffusion imaging in dynamic NMR microscopy, J. Magn. Reson. 91 (1991) 326–352.
[40] P.T. Callaghan, A simple matrix formalism for spin echo analysis of restricted diffusion under generalized gradient waveforms, J. Magn. Reson. 129 (1997) 74–84.
[41] E.O. Stejskal, J.E. Tanner, Spin diffusion measurements: spin echoes in the presence of a time-dependent field gradient, J. Chem. Phys. 42 (1965) 288–292.
[42] H.Y. Carr, E.M. Purcell, Effects of diffusion of free precession in nuclear magnetic resonance experiments, Phys. Rev. 94 (1954) 630–638.
[43] Available from <http://www.nmr.fhg.de/smile.shtm>.
[44] T. Gullion, D.B. Baker, M.S. Conradi, New, compensated Carr-Purcell sequences, J. Magn. Reson. 89 (1990) 479–484.
[45] R.V. Mulkern, S.T.S. Wong, P. Jakab, A.R. Bleier, T. Sandor, F.A. Jolesz, CPMG imaging sequences for high field in vivo transverse relaxation studies, Magn. Reson. Med. 16 (1990) 67–79.
[46] Y. Xia, P.T. Callaghan, K.J. Jeffrey, Imaging velocity profiles: flow through an abrupt contraction and expansion, AICHE J. 38 (1992) 1408–1420.
[47] B. Buhai, A. Hakimov, I. Ardelean, R. Kimmich, NMR acceleration mapping in percolation model objects, J. Magn. Reson. 168 (2004) 175–185.
[48] B. Rittman, The effect of shear stress on biofilm loss rate, Biotechnol. Bioeng. 24 (1982) 501–506.
[49] R. Bakke, M.G. Trulear, J.A. Robinson, W.G. Characklis, Activity of *Pseudomonas aeruginosa* in biofilms: steady state, Biotechnol. Bioeng. 26 (1984) 1418–1424.
[50] B.M. Peyton, W.G. Characklis, A statistical-analysis of the effect of substrate utilization and shear-stress on the kinetics of biofilm detachment, Biotechnol. Bioeng. 41 (1993) 728–735.
[51] G.T.Y. Wang, J.D. Bryers, A dymanic model for receptor-mediated specific adhesion of bacteria under uniform shear flow, Biofouling 11 (1997) 227–252.
[52] C. Picioreanu, M.C.M. van Loosdrecht, J.J. Heijnen, Two-dimensional model of biofilm detachment caused by internal stress from liquid flow, Biotechnol. Bioeng. 72 (2001) 205–218.
[53] H. Horn, H. Reiff, E. Morgenroth, Simulation of growth and detachment in biofilm systems under defined hydrodynamic conditions, Biotechnol. Bioeng. 81 (2003) 607–617.